# A simple method for evaluating and predicting chaotic advection in microfluidic slugs

Sivasamy Jayaprakash; Che, Zhizhao; Wong, Teck Neng; Nguyen, Nam-Trung; Yobas, Levent

2010

Sivasamy, J., Che, Z., Wong, T. N., Nguyen, N. T. & Yobas, L. (2010). A Simple Method for Evaluating and Predicting Chaotic Advection in Microfluidic Slugs. Chemical Engineering Science, 65(19), 5382–5391.

https://hdl.handle.net/10356/94663

https://doi.org/10.1016/j.ces.2010.06.017

# A simple method for evaluating and predicting chaotic advection in microfluidic slugs

*Jayaprakash Sivasamy [a,b], Zhizhao Che [a], Teck Neng Wong [a,*], Nam-Trung Nguyen [a], Levent Yobas [b]*

*a School of Mechanical and Aerospace Engineering, Nanyang Technological University, 50 Nanyang Avenue, Singapore 639798, Singapore*

*b Institute of Microelectronics, A*STAR (Agency for Science, Technology and Research), 11 Science Park Road, Singapore 117685, Singapore*

** Corresponding author.Tel.:+6567905587;fax:+6567911859.*

*E-mail address: mtnwong@ntu.edu.sg (T.N.Wong).*

**Abstract**

A simple method for evaluating chaotic advection in slug micromixing is reported in this paper. We consider a slug moving in a slit microchannel (w>> h) and flow field in a plane far from the boundary walls is modelled as a two-dimensional low-Reynolds-number flow (Stokes flow). Analytical solution for normalised velocity field in the slug is derived. The two-dimensional analytical solution is compared with the two-dimensional slice from the three-dimensional numerical solution of the slug velocity field. Boundary conditions mimicking the motion of the slugs in microchannel geometries, in Lagrangian frame of reference, is used to track the passive tracer particles using Lagrangian particle tracking method. Poincaré sections and dye advection patterns are used to analyse chaotic advection of passive tracer particles using statistical concepts such as 'variance', 'Shannon entrophy' and 'complete spatial randomness'. Results for boundary conditions mimicking constant-velocity straight-channel flow, constant-velocity normal-meandering channel flow are compared. A method for finding new channel geometries which enhance chaotic mixing is also proposed.

*Keywords:* Microfluidics; Micromixing; Chaotic advection; Slug; Droplet; Modelling

## 1. Introduction

In microscale, momentum, mass and energy transport experience laminar and Stokes flow conditions (i.e., low-Reynolds number, Re<1) (Manz et al., 1990; Whitesides, 2006). Unavailability of turbulent conditions make mixing dependent on the diffusive properties of the species involved in the process (Günther et al., 2004). In micro-total-analysis systems (μ—TAS), species involved in the analysis are macromolecules and biological species with low mass diffusivities and hence have long mixing time in laminar flow conditions. They are comprehensively reviewed by Nguyen and Wu (2005), Hardt et al. (2005) and Teh et al. (2008).

Droplet and gas–liquid segmented flow are the two kinds of flow that have been investigated for passive micromixing of liquids as they are known to mix the components rapidly by internal recirculation (Song et al., 2003a, b; Bringer et al., 2004; Garstecki et al.,

2006a, b; Tanthapanichakoon et al., 2006; Günther et al., 2004, 2005). Laminar flow conditions, which is prevalent in continuous microchannel flows, can be observed in droplet micromixing (Teh et al., 2008). In droplet flows, the liquid inside the droplet generates two counter rotating vortices. In the case of gas–liquid segmented flow, the liquid-slug between two gas bubbles generates the counter rotating vortices in the Taylor flow regime (Fries et al., 2008).

From the available literature (Aref, 1984, 2002; Stone et al., 2004), it is well understood that chaotic advection can be produced whenever the kinematic equations of motion for passively advected particles give rise to a nonintegrable dynamical system. Understanding the passive advection of particles in the complex laminar flow is considered as a useful first step in describing the mixing process in chaotic advection driven microscale mixing. Channel modifications have been implemented to improve the chaotic advection by promoting internal circulation of liquids in the vortices in droplets and slug. When a droplet moves through a straight microchannel, recirculating flow of equal size is generated in each half of the droplet (Handique and Burns, 2001). Fluids within each half of the droplet are mixed, but the two halves remain unmixed and separated from each other.

To enhance internal mixing within droplets, modifications in the channel geometry, by employing turns and bends, are used to create chaotic advection to fold and stretch the content of the droplet (Song et al., 2003b; Teh et al., 2008). As the droplet traverses through a curved channel, the two halves of the droplet experience unequal recirculating flows. One half of the droplet is exposed to the inner arc of the winding channel, a shorter channel section, and thus a small recirculating flow is generated compared to the other half of the droplet which is exposed to a longer channel section. The irregular motion along the walls promoted chaos and crossing of fluid streams since the vortices of each half are assymetrical. The sharp turns also help to reorient the droplet, so that it becomes thoroughly mixed as it goes through a series of stretching, reorientation, and folding (Bringer et al., 2004).

Many of the studies in microfluidics literature are application-driven experimental studies involving complex geometries with no theory (Shui et al., 2008). Very few researchers have tried to model the chaotic motion in slugs and droplets moving in microfluidic channels. Experimental scaling of the chaotic mixing in a droplet moving through a winding microfluidic channel has been done using baker's transformation (Song et al., 2003a). However, the argument was too simple and does not provide the optimization of the channel geometry for rapid mixing through chaotic advection. A mathematical model to estimate the mixing time for slugs in a straight slit microchannel was proposed (Handique and Burns, 2001). Although the model did estimate the time required for mixing, it did not provide any insight about chaotic motion in the slugs. The mixing characteristics inside a microfluidic slug using computational fluid dynamics was done by Tanthapanichakoon et al. (2006), where each slug was modelled as a single-phase flow domain in two-dimensional (2D) as well as in three-dimensional (3D) domain. Boundary conditions of the slug in Lagrangian frame of reference were used to simulate the mixing characteristics. They reported that the radially arranged reactants mix more rapidly than the axially arranged reactants and proposed a new dimensionless number to estimate mixing rates. However, they did not calculate chaotic advection of the flow inside the slugs. Since droplets and slugs produce similar vortices, similar inferences can be made from their flow fields when moving in various microchannel geometries and hence only the slug terminology will be used for convenience hereafter.

In order to understand mixing in microfluidic slugs, we propose a simple method to characterize the chaotic flow: Analytical solution for the two-dimensional flow field is derived and the boundary conditions mimicking the flow of the slug in microchannel are used to get the velocity at every point of the flow domain. Velocity field obtained from the analytical model is used to track the passive tracer particles and construct Poincarė maps and dye advection pattern. To analyse the nature of chaotic advection, traditional tools such as 'variance', 'Shannon entrophy' and 'complete spatial randomness' are used. Based on the 2D model and the results obtained, a method to predict microchannel geometries which can produce chaotic advection in liquid-slug and droplet flows is proposed.

## 2. Problem description

Microchannel flows are similar to Stokes flow problems because of the inherently laminar flow conditions. Gas–liquid segmented flow (often called as slug flow) can be described by Stokes equations, when the liquid-slug is considered as a single-phase flow in Lagrangian frame of reference, which model viscous fluids in macroscales and ordinary fluids in microscales. We consider the case where a slug fully occupies the channel cross-section and its cross-sectional shape is determined by that of the channel. The microchannel is considered as infinitely large in one of the three directions and therefore the flow in a plane far from the boundary walls, in the direction, is two-dimensional. Fig. 1 shows the model of a liquid-slug with moving wall boundary conditions in Lagrangian frame of reference in a straight rectangular microchannel. The continuous phase is assumed to wet the wall well and no-slip condition is applied on the top and the bottom of the slug. In the front and the rear, the slug is surrounded by an immiscible phase with negligible viscosity such as air and therefore no shear stress condition is assumed. Other assumptions made in this analysis are: no body force has any influence on the slug; the slug is approximately rectangular; the liquid in the slug is an incompressible Newtonian fluid. Two-dimensional flow field numerically simulated by Fluent (ANSYS, Inc., USA) is used to compare the analytical results in the next section.

## 3. Modelling

### *3.1. 2D analytical solution*

Following the works of Shankar (2007) and Timoshenko (1951), the governing equation for Stokes flow in the slug can be simplified as a biharmonic equation. Using the finite Fourier transform (FFT) method, the dimensionless velocities in the x and z directions can be obtained as follows (for details see Appendix):

$$\hat{u}_x = \frac{\partial}{\partial z}\hat{\varphi}(\hat{x},\hat{z}) = \sum_{n=1}^{\infty} \sin(\alpha_n \hat{x}) \times [C_{1n}\alpha_n \sinh(\alpha_n \hat{z}) + C_{2n}\alpha_n \cosh(\alpha_n \hat{z}) + C_{3n}\alpha_n \hat{z}\sinh(\alpha_n \hat{z}) + C_{3n}\cosh(\alpha_n \hat{z}) + C_{4n}\alpha_n \hat{z}\cosh(\alpha_n \hat{z}) + C_{4n}\sinh(\alpha_n \hat{z})] \quad (1)$$

$$\hat{u}_z = -\frac{\partial}{\partial x}\hat{\varphi}(\hat{x},\hat{z}) = -\sum_{n=1}^{\infty}\cos(\alpha_n\hat{x}) \times[C_{1n}\cosh(\alpha_n\hat{z}) + C_{2n}\sinh(\alpha_n\hat{z}) + C_{3n}\hat{z}\cosh(\alpha_n\hat{z}) + C_{4n}\hat{z}\sinh(\alpha_n\hat{z})] \quad (2)$$

The constant coefficients are

$$C_{1n} = 0 \quad (3)$$

$$C_{2n} = -\frac{4\xi}{D_n\beta\alpha_n}\sinh(\alpha_n) + \frac{4\eta}{D_n\beta}[\sinh^2(\alpha_n) - \cosh^2(\alpha_n)] \quad (4)$$

$$C_{3n} = \frac{4\xi}{D_n\beta}\sinh(\alpha_n) + \frac{4\eta\sinh^2(\alpha_n)}{\beta\alpha_n D_n} \quad (5)$$

$$C_{4n} = \frac{4\xi}{D_n\beta\alpha_n}[-\alpha_n\cosh(\alpha_n) + \sinh(\alpha_n)] + \frac{4\xi}{D_n\beta\alpha_n}[-\sinh(\alpha_n)\cosh(\alpha_n) - \alpha_n\sinh^2(\alpha_n) + \alpha_n\cosh^2(\alpha_n)] \quad (6)$$

where

$$D_n = \alpha_n^2\cosh^2(\alpha_n) - (\alpha_n^2 + 1)\sinh^2(\alpha_n) \quad (7)$$

*3.2. 3D numerical simulation*

To verify the validity of the model described above, the analytical flow field is compared with the numerically simulated flow field using the commercial CFD software Fluent 6.3.26 (ANSYS, Inc., USA). The dimensions of the slug taken for the simulation are 100 x 200 x 50μm in x, y and z directions, respectively. Therefore, l: w: h of the slug is 2:4:1 and in x–z directions, the 2D plane in consideration is of the ratio 2:1. The front and rear end of the slug are assumed to be straight edges, as the effect of the edge curvatures is small (Tanthapanichakoon et al., 2006). Steady-state simulation condition was assumed. The number of meshes used for the simulation was 64000. The mesh independence was confirmed. The density and viscosity were set at 998.2 kg/m$^3$ and 0.001 Pa s, respectively, as water is taken as the operating fluid. Since the Reynolds number is very low in the microfluidic slugs, the laminar flow model was used. The moving wall boundary conditions for all the four walls were set at 5 mm/s and for the front and the rear ends, no shear wall conditions were applied. Convergence criteria for x, y and z velocity values were set at $10^{-5}$. Slices of the three-dimensional numerical simulation of the flow field inside the slug is shown in Fig. 2. The contour slices are showing the flow field in the x–z planes from wall to wall in the Y-axis.

*3.3. Comparison*

For comparing the analytical flow field with the numerically computed flow field, we take the flow field at the middle plane, which is far from the boundary walls. Therefore, numerical velocity flow field from the plane in the y-axis at y= 0.0001 m (100μm) was taken for comparison.

Flow field for both analytical and numerical solution is shown in Figs. 3(a) and (b), respectively. For the analytical velocity flow field, the moving wall velocity boundary conditions on the top ($U_{top}$) and the bottom ($U_{bottom}$) of the slug are both 5 mm/s and the aspect ratio of the slug is 2, which are same as used for numerical simulation. As seen in Figs. 3(a) and (b), both analytical and numerical flow field contours and the velocity vectors are similar. To make sure that they are of the same magnitude, velocity profiles at three different positions along x-axis are compared. Velocity profile plots of analytical and numerical flow fields at $\frac{1}{4}$, $\frac{1}{2}$ and $\frac{3}{4}$ positions of the slug are shown in Fig. 4. The continuous outer x-axis in Fig. 4 stands for the position on the slug, where the velocity profile is drawn and the three discrete inner x-axis stand for the magnitude of the velocity in that particular position of the slug. As seen in Fig. 4, both analytical and numerical velocity profiles are of the same magnitude with little variation in the center. Therefore, the 2D simplification of the flow field for the slug flow in slit microchannel is valid and can be used to analyse the chaotic advection by tracking passive tracer particles in the slug.

## 4. Particle tracking

In this study, we use passive massless tracers to construct the particle trajectories in the flow domain using Lagrangian particle tracking method. The velocity expression $\dot{x} = v(x,t)$ is used for the integration, where *x* is the position vector, *v* is the velocity, *t* is the time, and the dot denotes a material derivative. Here, we use only the analytically known Eulerian velocity field, therefore the integration can be carried out by the standard fourth order Runge–Kutta method. Boundary conditions used for finding the analytical velocity field, which is used to track the particles in the slugs, are discussed in the next section. The constant integration time, Δt = 0.02 s, was found by running a few trials of computation for the range of boundary wall velocities used in this study. The choice of integration time Δt is dictated by (1) the accuracy of tracing the particle along the streamline in a non-chaotic flow field without moving out of it, i.e., the particle has to simply trace the streamline pattern, (2) the highest among the values, to avoid the need for huge computational resources.

*4.1. Boundary conditions*

Analytical velocity flow fields, for tracking passive tracer particles, were found by using the boundary conditions which mimic the kind of motion the slug undergoes in microchannels. For straight microchannels, the slug experiences a constant velocity on the walls in Lagrangian frame of reference. Therefore a constant velocity of -5 mm/s was used in Eq. (1), along with the constant coefficients for finding the velocity flow field. Though the slug is moving in the positive x-direction, the velocity boundary condition is negative because the frame of reference is moving with the slug. For meandering microchannel, in the first half period, the outer wall moves at a higher speed ($V_{R1}$) and inner wall moves at a lower speed ($V_{R2}$). In the second half, the wall velocities reverse. Effect of change in the wall

velocity reflects in the size of the vortices formed in the slug as shown in Fig. 5(a). Boundary conditions mimicking the motion of the slug through the meandering channel and the straight channel for a single period are shown in Fig. 5(b). The difference between the wall velocities is dependent on the dimensions of the microchannel such as radius, width and the angular velocity of the slug. The outer radius, inner radius and width of the channel are 1000, 800 and 200 μm, respectively. Angular velocity of the slug is ω= 1 rad/s. The inner and outer wall velocities were calculated from the relation, $V_S = (V_{R1} + V_{R2})/ 2$, where $V_S$ is the straight channel wall velocity.

## 5. Chaotic advection evaluation

### *5.1. Poincaré map*

Poincaré map, a Lagrangian tool constructed by recording the particle positions for long time, is used to evaluate the advective transport of fluid particles. The disposition of the particle positions in Poincarémap reveals the nature of the flow: chaotic nature of the flow field appears as randomly distributed; non-chaotic flow appears as islands or closed curves (Aref, 1984, 2002). Since we use massless tracer particles, when the flow is steady, the particle trajectories correspond to stream lines and hence no chaotic advection. Fig. 6(a) is the Poincaré map for straight channel velocity boundary condition, which shows that particles move in closed curves.

When the flow is unsteady and chaotic, stretching and folding of fluid elements occur and produces an exponential growth of the fluid interface and the particle positions are randomly distributed. In this study, Poincaré sections are obtained by following the motion of 20 material points, which are put in a group at the location (1.4, 0.4) in a slug for the aspect ratio of 2, for the duration of 2000 periods. An impression of the poincaré sections that have been found for the straight micro channel and the meandering microchannel can been seen in Figs. 6(a) and (b), respectively.

### *5.2. Construction of dye advection pattern maps*

Advection pattern of massless passive tracers are obtained by tracking the positions of 20,000 material points which are initially concentrated in a rectangular box of size 0.05 x 0.05 centered at the point (1.45, 0.45). Blue and red colour particles are used to distinguish the upper and lower half particles in the rectangular box similar to the work by Kang and Kwon (2004) and it is useful to visually identify the globally chaotic flow. In this study, 40 periods of meandering channel boundary conditions with 630 iterations per period are used to track the particles in the slug. Particle positions were recorded at the end of each period of tracking to see the particle advection patterns. Figs. 7(a–f) show the dye advection patterns for the slug of aspect ratio 2 for periods from 1 to 40 with interval of 8 periods.

## 6. Results and discussion

### *6.1. Characterizing of chaotic mixing*

To calculate the mixing efficiency, we use the popular tools such as ‘variance index ($I_{var}$)’, ‘Shannon entrophy index ($I_S$)’ and ‘complete spatial randomness (CSR)’. Variance as a mixing measure has been widely used to characterize the chaotic mixing along with Shannon entrophy index (Phelps and TuckerIII, 2006). Variance of the particle counts in the bins is

calculated by dividing the whole flow domain into n x m grid of equal-size bins. The variance $\sigma^2$ is calculated as

$$\sigma^2 = \frac{1}{M}\sum_{j=1}^{M}(c_j - \overline{c})^2 \tag{8}$$

where M is the number of bins and $c_j$ is the number of particles in bin j, $\overline{c}$ is the average number of particles per bin, $\overline{c} = N/M$, with N the total number of particles in the calculation. The variance decreases with the number of periods as mixing improves, and particles are distributed in the computational domain. Variance index, which varies from unity to zero and allows easy comparison of mixing calculations, is defined as

$$I_{var} = \frac{\sigma^2}{\sigma_0^2} \tag{9}$$

where $\sigma^2$ denotes the most segregated state which can be deduced from Eq. (8) as $\sigma^2 \approx N^2/M$, when M >>1. Shannon entrophy, S, another measure used to analyse chaotic mixing widely, is defined as

$$S = -\sum_{j=1}^{M} p_j \ln p_j \tag{10}$$

where $p_j$ is the probability that a particle will lie in bin j. With Lagrangian particle method, the probability is taken as the particle count in a bin divided by the total number of particles, or $p_j = cj/N$. Shannon entrophy index $I_S$ is defined as

$$I_S = 1 - \frac{S}{S_e} \tag{11}$$

where Se is the condition of even distribution of particles and each bin has an equal probability 1/M and the corresponding entrophy is Se= ln M. This form of the normalization makes it easy to see the details as a mixture approaches uniformity, by plotting $I_S$ on a logarithmic scale.

Complete spatial randomness (CSR), which is the even distribution of material points through out the flow domain, is taken as the measure of complete mixing. This is an ideal state for a physical mixture. However, in Lagrangian particle tracking method, repeated iterations of a globally chaotic flow do not result in an even distribution of the particles, but rather one in which each particle is equally likely to lie in any bin.

According to the binomial probability mass function (PMF) of the bin counts, for M >>1 and N >>1 the binomial PMF asymptotes to the Poisson PMF,

$$p(c) = \left(\frac{N}{M}\right)^{c} \frac{e^{N/M}}{c!} \tag{12}$$

with a variance of $\sigma^2_{CSR}$= N/M and this gives the CSR limit for variance index $I_{var,CSR}$=1/N and for the entrophy index the limit is $I_{S,CSR}$= M/2N ln(M). Once a random distribution of particles throughout the flow is achieved, the limiting values of variance and Shannon entrophy index are reached. CSR is a fundamental numerical limit for any Lagrangian particle calculation and no further distribution of particle can be attained. Details of the above discussion on ($I_{var}$), ($I_S$) and CSR is referred to the work by Phelps and TuckerIII (2006).

As seen in Fig. 6(a), Poincaré map constructed for straight channel shows that the particles in the slug move along with streamlines. This is because of the velocity flow field for constant wall velocity boundary on the slug that produces two vortices with symmetrical recirculation along the channel centerline. In a simple non-chaotic recirculating flow field, particles can

move from one half to the other can happen only through diffusion. And the particles used for particle tracking in this study are passive massless tracers with zero diffusivity and therefore they simply follow the flow field.

Poincaré map for meandering channel flow is seen in Fig. 6(b) and the particles are evenly distributed throughout the domain. Using the traditional approach of visually analyzing Poincaré sections shows that there are no islands and can be classified as globally chaotic flow. Total number of particles in the Poincaré map is 40,000 which exceeds the requirement of sufficient number particle positions, n > MIn(M)=5348, for evaluating Poincaré maps, (Phelps and TuckerIII,2006), where the number of bins M=800. Fig.8 shows the 'variance index' and 'Shannon entropy index' for the dye advection patterns, as seen in Fig. 7. computed for the slug from velocity flow field obtained for the meandering channel flow. Both mixing measures show that the mixing is complete and approach the state of 'complete spatial randomness'. Therefore, it is clear that the meandering channel geometry is useful in chaotic mixing due to its ability to create assymetrical vortices.

*6.2. Predicting a channel geometry for chaotic mixing*

As described above in Section 4.1, wall velocity boundary conditions applied on the walls of the slug is determined by the channel geometry in which the slug is moving as seen in Fig. 5. Therefore, the two-dimensional model in Section 3 can be used along with the boundary conditions for a particular channel geometry to identify the channel geometry which enhances chaotic mixing in the slug, by tracking particles in the velocity As described above in Section 4.1, wall velocity boundary conditions applied on the walls of the slug is determined by the channel geometry in which the slug is moving as seen in Fig. 5. Therefore, the two-dimensional model in Section 3 can be used along with the boundary conditions for a particular channel geometry to identify the channel geometry which enhances chaotic mixing in the slug, by tracking particles in the velocity

## 7. Conclusions

We have proposed a simple 2D analytical model for evaluating and predicting chaotic advection in slug flow in high aspect ratio microchannels. The velocity flow field of the 2D analytical equations was validated against a 2D slice of the 3D numerical velocity flow field and it showed that the 2D model is good enough to represent the flow field in the center of the droplet and slugs flowing in high aspect ratio channels. Boundary conditions mimicking the motion of the slugs in straight channel and meandering channels have been applied to get the velocity flow fields in the slugs.

Lagrangian particle tracking has been used to compute Poincaré maps and dye advection patterns of passive tracer particles. Poincaré maps and dye advection patterns were analysed using the statistical tools such as 'variance index', 'Shannon entrophy index' and 'complete spatial randomness'. The analysis shows that the slug flow in high aspect ratio meandering channel flow could produce chaotic advection because of the change in the size of the vortices due to the curvature of the channel. A method of applying corresponding boundary conditions for a channel geometry has been proposed, to find a new channel goemetries and motion of the slugs and droplets, which could produce chaotic advection.

**Acknowledgements**

The authors would like to thank the Agency of Science Technology and Research, Singapore, A*star, SERC Grant no. 0521010108 'Droplet-based micro/nanofluidics' for its financial support.

## Appendix A

For the Stokes flow in the slug, the governing equation is biharmonic

$$\nabla^4 \varphi = 0 \tag{A.1}$$

where φ is the stream function, which is defined as

$$u_x = \frac{\partial \varphi}{\partial z}; \quad u_z = -\frac{\partial \varphi}{\partial x} \tag{A.2}$$

This definition of φ satisfies the continuity equation automatically. The stream function is constant on the boundaries. Here, we set it to be zero.

$$\varphi(0,z) = 0; \quad \varphi(L,z) = 0; \quad \varphi(x,0) = 0; \quad \varphi(x,h) = 0 \tag{A.3}$$

The two ends of the slug are considered as free surfaces, because the viscous of the air is neglected. The boundary conditions at these two ends are, respectively,

$$\frac{\partial^2}{\partial x^2}\varphi(0,z) = 0; \quad \frac{\partial^2}{\partial z^2}\varphi(L,z) = 0 \tag{A.4}$$

The velocities at the outer and the inner sides walls are –S' and –S respectively

$$\frac{\partial}{\partial z}\varphi(x,0) = -S'; \quad \frac{\partial}{\partial z}\varphi(x,h) = -S \tag{A.5}$$

*A.1. Nondimensionalization*

Using the height of the channel h and the velocity of the wall Vs to nondimensionalize x,z,φ

$$\hat{x} \equiv x/h; \quad \hat{z} \equiv z/h; \quad \hat{u}_x \equiv u_x/V_s; \quad \hat{u}_z \equiv u_z/V_s; \quad \hat{\varphi}_z \equiv \varphi/(hV_s) \tag{A.6}$$

The dimensionless governing equation is

$$\left(\frac{\partial^4}{\partial \hat{x}^4} + 2\frac{\partial^4}{\partial \hat{x}^2 \partial \hat{z}^2} + \frac{\partial^4}{\partial \hat{z}^4}\right)\hat{\varphi} = 0 \tag{A.7}$$

and the dimensionless boundary conditions are, respectively,

$$\hat{\varphi}(0,\hat{z}) = 0; \quad \hat{\varphi}(\beta,\hat{z}) = 0 \tag{A.8}$$

$$\hat{\varphi}(\hat{x},0) = 0; \quad \hat{\varphi}(\hat{x},1) = 0; \quad \frac{\partial^2}{\partial \hat{x}^2}\hat{\varphi}(0,\hat{z}) = 0; \quad \frac{\partial^2}{\partial \hat{x}^2}\hat{\varphi}(\beta,\hat{z}) = 0 \tag{A.9}$$

$$\frac{\partial}{\partial \hat{z}}\hat{\varphi}(\hat{x},0) = -\eta; \quad \frac{\partial}{\partial \hat{z}}\hat{\varphi}(\hat{x},1) = -\xi \tag{A.10}$$

where β=L/ h is the aspect ratio; ŋ =S'/ Vs and ξ=S/ Vs are dimensionless velocities at the walls of the channel.

*A.2. Analytical solution*

Using the finite Fourier transform (FFT) method, the solution of the biharmonic equation can be written as

$$\hat{\varphi}(\hat{x},\hat{z}) = \sum_{n=0}^{\infty}[\varphi_n(\hat{z})\sin(\alpha_n\hat{x}) + \psi_n(\hat{z})\cos(\alpha_n\hat{x})] \tag{A.11}$$

which is the Fourier transform of $\hat{\varphi}(\hat{x},\hat{z})$, where $\alpha_n = n\pi/\beta$. According to the boundary conditions (A.9), the solution can be written in a simpler format

$$\hat{\varphi}(\hat{x},\hat{z}) = \sum_{n=1}^{\infty} \varphi_n(\hat{z})\sin(\alpha_n\hat{x}) \tag{A.12}$$

Using the FFT method, the dimensionless stream function φ can be determined as

$$\begin{aligned}\hat{\varphi}(\hat{x},\hat{z}) = \sum_{n=1}^{\infty} & \sin(\alpha_n\hat{x}) \\ & \times(C_{1n}\cosh(\alpha_n\hat{z}) + C_{2n}\sinh(\alpha_n\hat{z}) \\ & + C_{3n}\hat{z}\cosh(\alpha_n\hat{z}) + C_{4n}\hat{z}\sinh(\alpha_n\hat{z}))\end{aligned} \tag{A.13}$$

Therefore, the dimensionless velocity components in the $\hat{x}$ and $\hat{z}$ directions are, respectively,

$$\begin{aligned}\hat{u}_x = \frac{\partial}{\partial z}\hat{\varphi}(\hat{x},\hat{z}) = \sum_{n=1}^{\infty} & \sin(\alpha_n\hat{x}) \\ & \times[C_{1n}\alpha_n\sinh(\alpha_n\hat{z}) + C_{2n}\alpha_n\cosh(\alpha_n\hat{z}) + C_{3n}\alpha_n\hat{z}\sinh(\alpha_n\hat{z}) \\ & + C_{3n}\cosh(\alpha_n\hat{z}) + C_{4n}\alpha_n\hat{z}\cosh(\alpha_n\hat{z}) + C_{4n}\sinh(\alpha_n\hat{z})]\end{aligned} \tag{A.14}$$

$$\begin{aligned}\hat{u}_z = -\frac{\partial}{\partial x}\hat{\varphi}(\hat{x},\hat{z}) = -\sum_{n=1}^{\infty} & \cos(\alpha_n\hat{x}) \\ & \times(C_{1n}\cosh(\alpha_n\hat{z}) + C_{2n}\sinh(\alpha_n\hat{z}) \\ & + C_{3n}\hat{z}\cosh(\alpha_n\hat{z}) + C_{4n}\hat{z}\sinh(\alpha_n\hat{z}))\end{aligned} \tag{A.15}$$

The constant coefficients can be determined from the boundary conditions Eqs. (A.8) and (A.10),

$$C_{1n} = 0 \tag{A.16}$$

$$C_{2n} = -\frac{4\xi}{D_n\beta\alpha_n}\sinh(\alpha_n) + \frac{4\eta}{D_n\beta}[\sinh^2(\alpha_n) - \cosh^2(\alpha_n)] \tag{A.17}$$

$$C_{3n} = \frac{4\xi}{D_n\beta}\sinh(\alpha_n) + \frac{4\eta\sinh^2(\alpha_n)}{\beta\alpha_n D_n} \tag{A.18}$$

$$\begin{aligned}C_{4n} = & \frac{4\xi}{D_n\beta\alpha_n}[-\alpha_n\cosh(\alpha_n) + \sinh(\alpha_n)] \\ & + \frac{4\xi}{D_n\beta\alpha_n}[-\sinh(\alpha_n)\cosh(\alpha_n) - \alpha_n\sinh^2(\alpha_n) + \alpha_n\cosh^2(\alpha_n)]\end{aligned} \tag{A.19}$$

Where

$$D_n = \alpha_n^2\cosh^2(\alpha_n) - (\alpha_n^2 + 1)\sinh^2(\alpha_n) \tag{A.20}$$

## References


[1] Aref, H., 1984. Stirring by chaotic advection. *Journal of Fluid Mechanics* 143, 1–21. Aref, H., 2002. The development of chaotic advection. Physics of Fluids 14 (4), 1315–1325.

[2] Bringer, M.R., Gerdts, C.J., Song, H., Tice, J.D., Ismagilov, R.F., 2004. Microfluidic systems for chemical kinetics that rely on chaotic mixing in droplets. *Philosophical Transactions of the Royal Society A: Mathematical, Physical and Engineering Sciences* 362 (1818), 1087–1104.

[3] Fries, D.M., Waelchli, S., von Rohr, P.R., 2008. Gas–liquid two-phase flow in meandering microchannels. *Chemical Engineering Journal* 135S, S37–S45.

[4] Garstecki, P., Fuerstman, M.J., Fischbach, M.A., Sia, S.K., Whitesides, G.M., 2006a. Mixing with bubbles: a practical technology for use with portable microfluidic devices. *Lab on a Chip* 6, 207–212.

[5] Garstecki, P., Fuerstman, M.J., Stone, H.A., Whitesides, G.M., 2006b. Formation of droplets and bubbles in a microfluidic T-junction—scaling and mechanism of break-up. *Lab on a Chip* 6 (3), 437–446.

[6] Günther, A., Jhunjhunwala, M., Thalmann, M., Schmidt, M.A., Jensen, K.F., 2005. Micromixing of miscible liquids in segmented gas–liquid flow. *Langmuir 21*, 1547–1555.

[7] Günther, A., Khan, S.A., Thalmann, M., Traschel, F., Jensen, K., 2004. Transport and reaction in microscale segmented gas–liquid flow. *Lab on a Chip 4*, 278–286.

[8] Handique, K., Burns, M.A., 2001. Mathematical modeling of drop mixing in a slit-type microchannel. *Journal of Micromechanics and Microengineering* 11 (5), 548–554.

[9] Hardt, S., Drese, K.S., Hessel, V., Schönfeld, F., 2005. Passive micromixers for applications in the microreactor and il-TAS fields. *Microfluidics and Nano-fluidics* 1, 108–118.

[10] Kang, T.G., Kwon, T.H., 2004. Colored particle tracking method for mixing analysis of chaotic micromixers. *Journal of Miromechanics and Microengineering* 14, 891–899.

[11] Manz, A., Graber, N., Widmer, H.M., 1990. Miniaturized total chemical analysis systems: a novel concept for chemical sensing. *Sensors and Actuators*: B. Chemical 1 (1–6), 244–248.

[12] Nguyen, N.-T., Wu, Z., 2005. Micromixers-a review. *Journal of Micromechanics and Microengineering* 15, R1–R16.

[13] Phelps, J.H.L., TuckerIII, C., 2006. Lagrangian particle calculations of distributive mixing: limitations and applications. *Chemical Engineering Science* 61, 6826–6836.

[14] Shankar, P., 2007. Slow Viscous Flows-Qualitative Features and Quantitative Analysis Using Complex Eigenfunction Expansions. *Imperial College Press*.

[15] Shui, L., Pennathur, S., Eijkel, J.C.T., van den Berg, A., 2008. Multiphase flow in lab on chip devices: a real tool for the future? *Lab on a Chip* 8, 1010–1014.

[16] Song, H., Bringer, M.R., Tice, J.D., Gerdts, C.J., 2003a. Experimental test of scaling of mixing by chaotic advection in droplets moving through microfluidic channels. *Applied Physics Letters* 83 (22), 4664–4666.

[17] Song, H., Tice, J.D., Ismagilov, R.F., 2003b. A microfluidic system for controlling reaction networks in time. *Angewandte Chemie-International Edition* 42 (7), 768–772.

[18] Stone, H.A., Ströock, A.D., Ajdari, A., 2004. Engineering flows in small devices: microfluidics toward a lab-on-a-chip. *Annual Review of Fluid Mechanics* 36, 381–411.

[19] Tanthapanichakoon, W., Aoki, N., Matsuyama, K., Mae, K., 2006. Design of mixing in microfluidic liquid slugs based on a new dimensionless number for precise reaction and mixing operations. *Chemical Engineering Science* 61, 4220–4232.

[20] Teh, S.-Y., Lin, R., Hung, L.-H., Lee, A.P., 2008. Droplet microfluidics. *Lab on a Chip 8* (2), 198–220.

[21] Timoshenko, S., 1951. Theory of Elasticity, second ed. McGraw-Hill, New York.

[22] Whitesides, G.M., 2006. The origins and the future of microfluidics. *Nature* 442

**List of Figures**

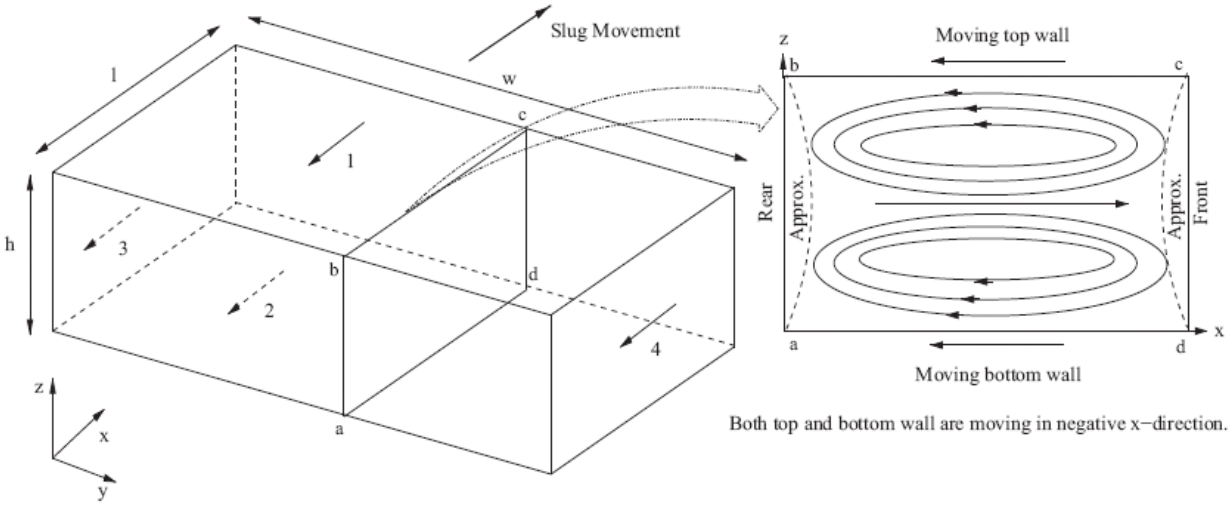


1. Moving top wall 2. Moving bottom wall 3. Moving side wall (outer) 4. Moving side wall (inner)

a b

Fig. 1

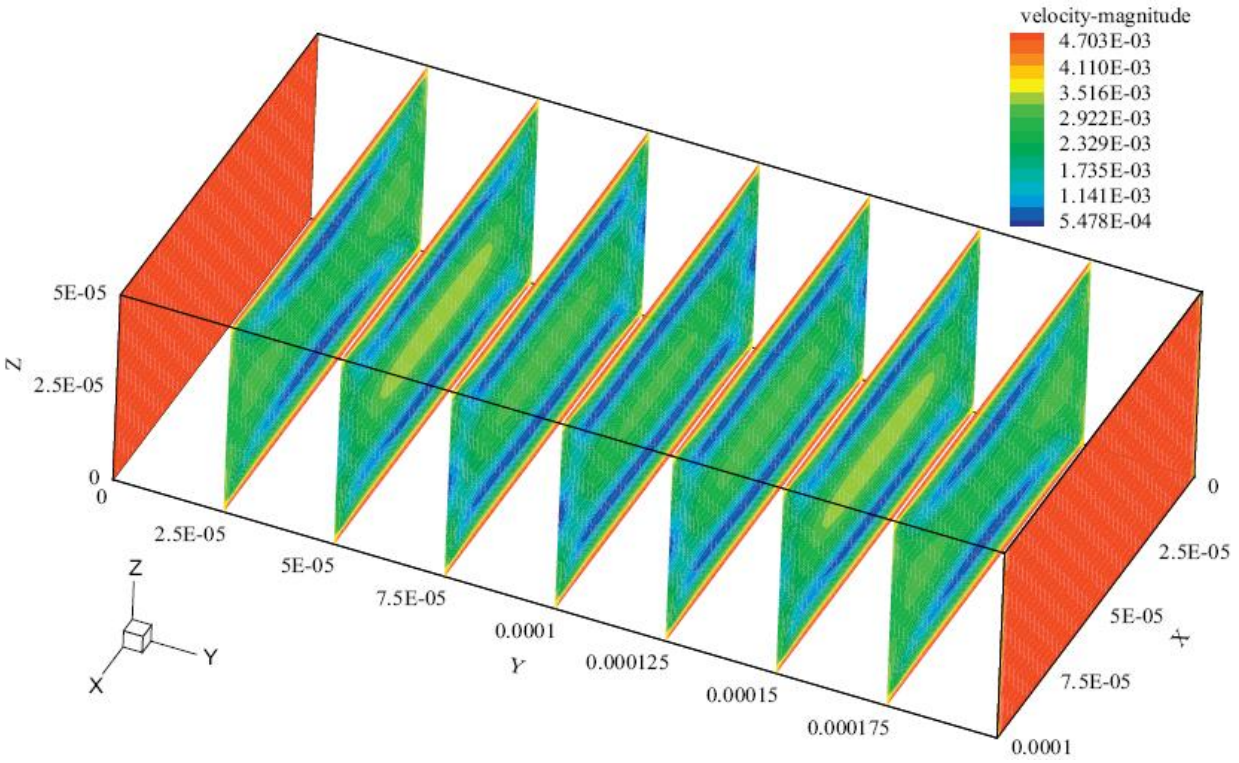
velocity-magnitude
4.703E-03
4.110E-03
3.516E-03
2.922E-03
2.329E-03
1.735E-03
1.141E-03
5.478E-04
Z
5E-05
2.5E-05
0
0
2.5E-05
5E-05
7.5E-05
0.0001
Y
0.000125
0.00015
0.000175
0.0001
7.5E-05
5E-05
2.5E-05
0
Z
Y
X

Fig. 2

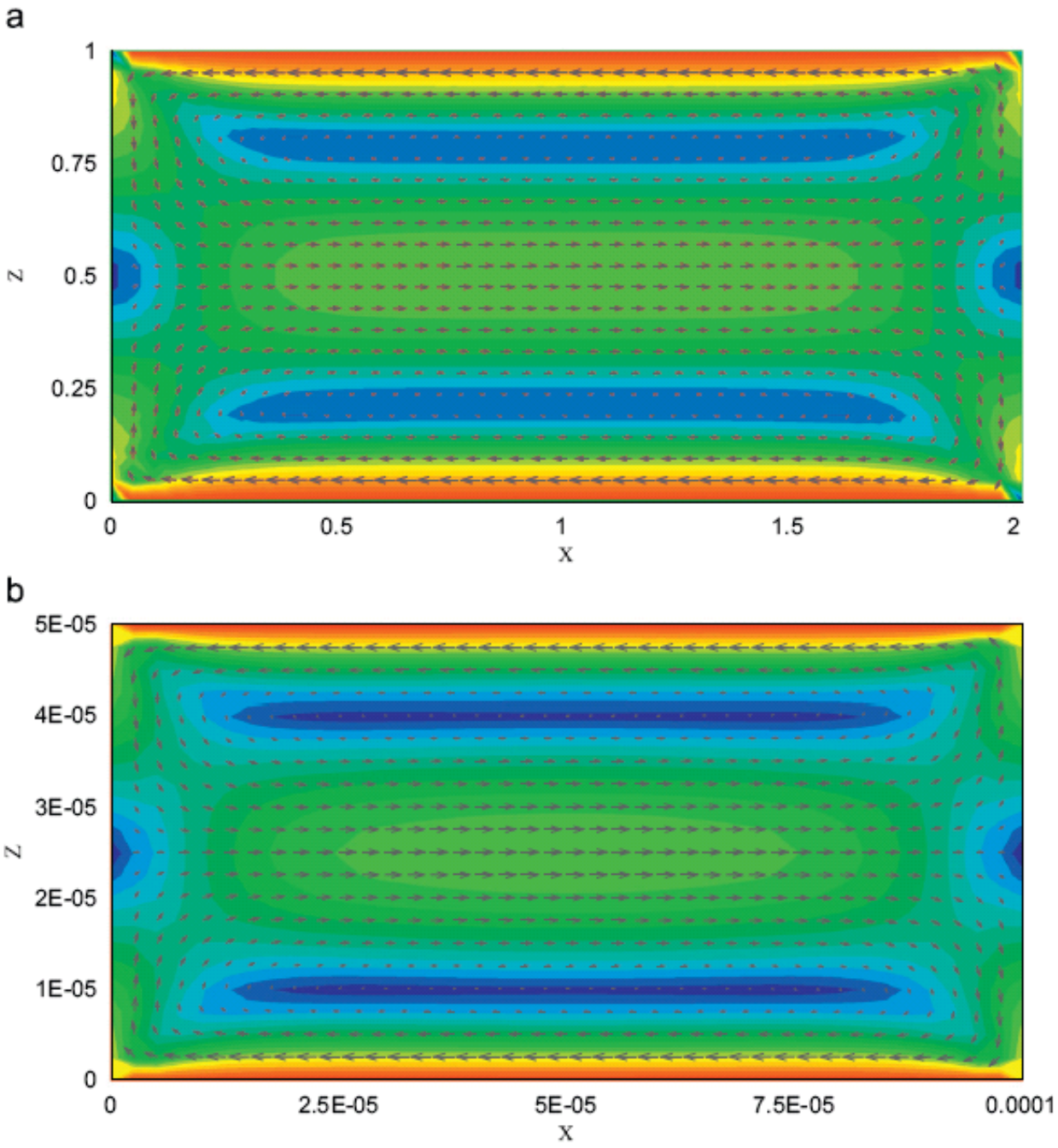
a
1
0.75
0.5
0.25
0
Z
0
0.5
1
1.5
2
X
b
5E-05
4E-05
3E-05
2E-05
1E-05
0
Z
0
2.5E-05
5E-05
7.5E-05
0.0001
X

Fig. 3

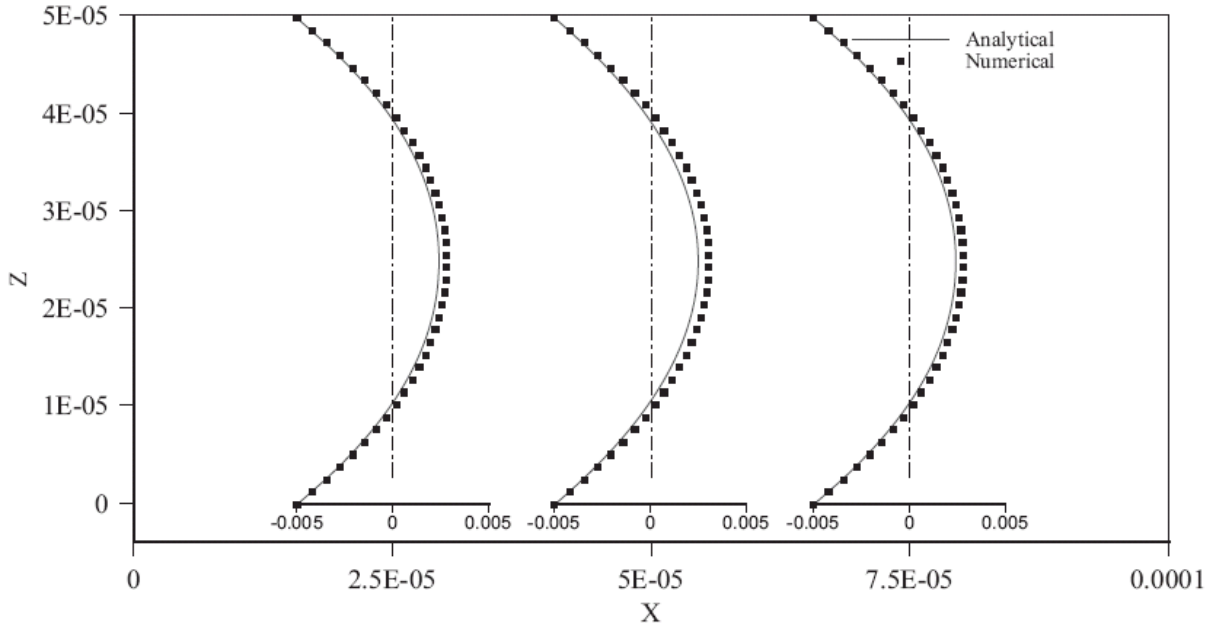
5E-05
4E-05
3E-05
2E-05
1E-05
0
Z
Analytical
Numerical
-0.005
0
0.005
-0.005
0
0.005
-0.005
0
0.005
0
2.5E-05
5E-05
7.5E-05
0.0001
X

Fig. 4

a

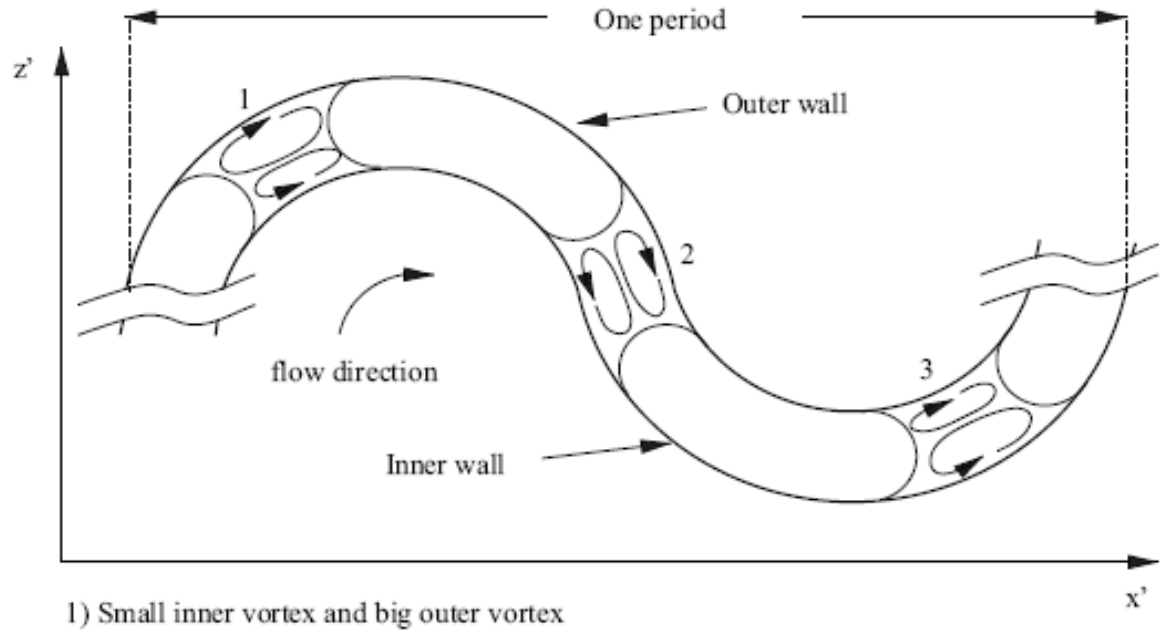


1) Small inner vortex and big outer vortex

2) Equal size vortices

3) Small outer vortex and big inner vortex

b

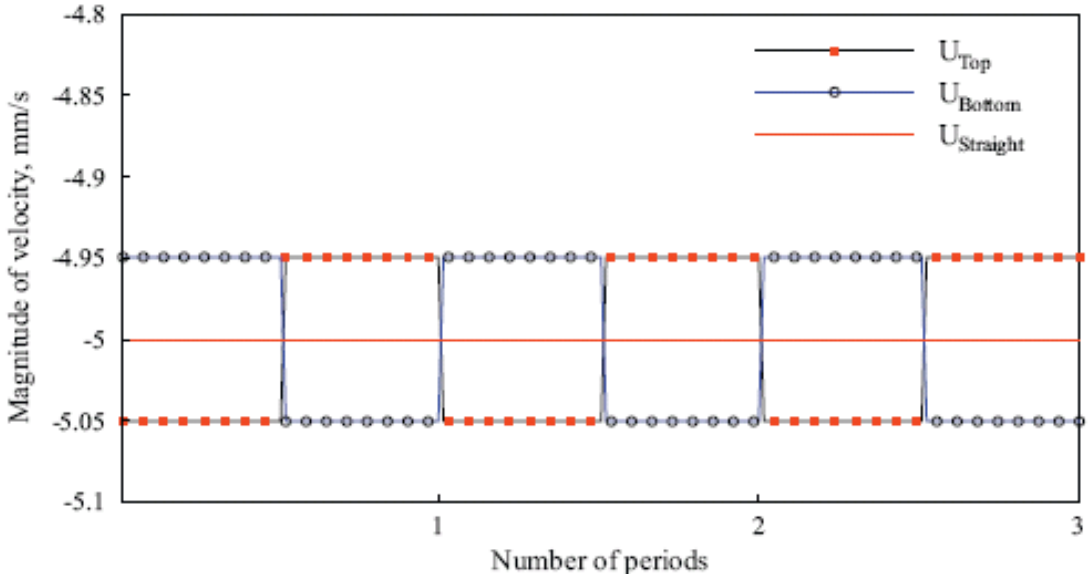


Fig. 5

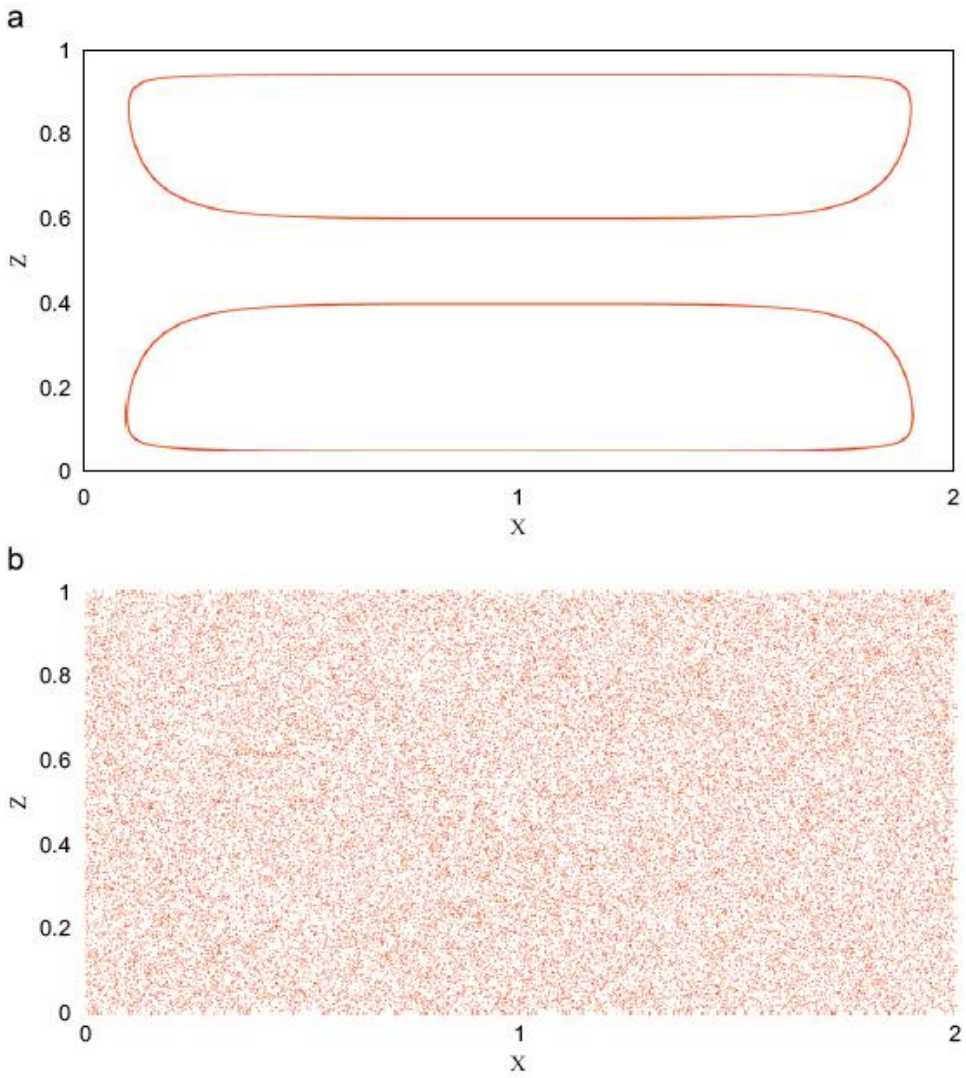


Fig. 6

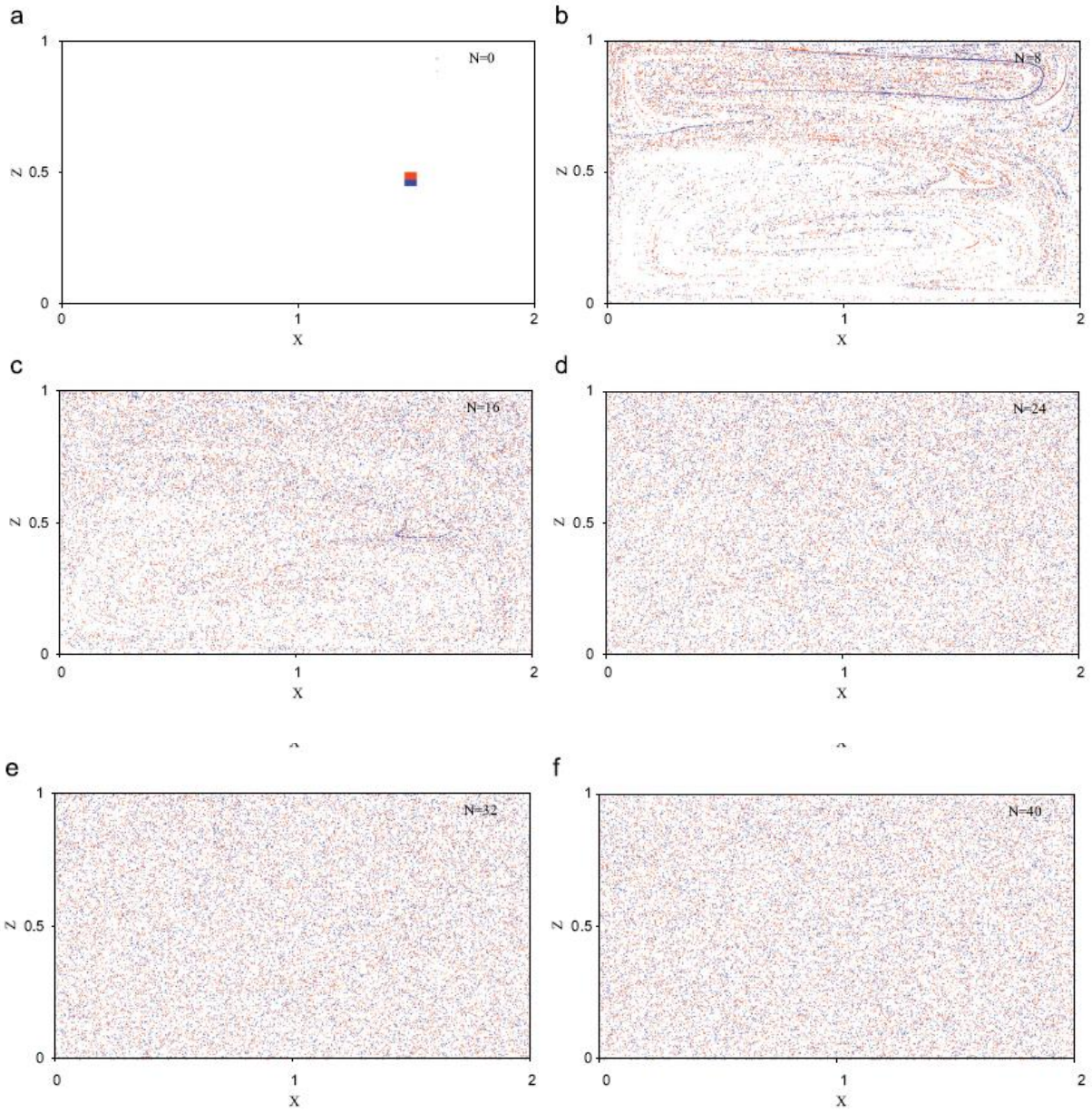


Fig. 7

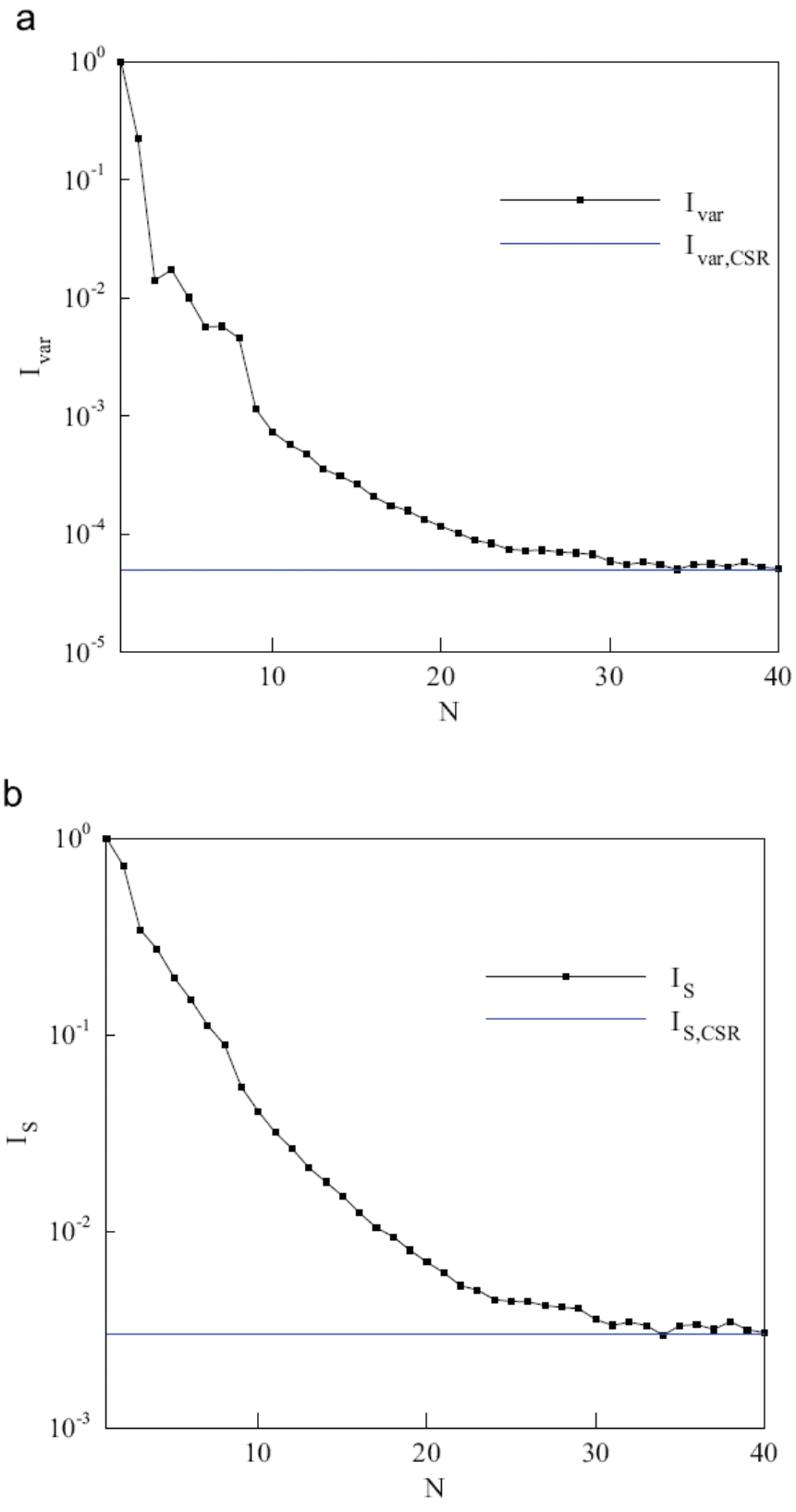
a
$10^0$
$10^{-1}$
$10^{-2}$
$10^{-3}$
$10^{-4}$
$10^{-5}$
$I_{var}$
$I_{var}$
$I_{var,CSR}$
10
20
30
40
N
b
$10^0$
$10^{-1}$
$10^{-2}$
$10^{-3}$
$I_S$
$I_S$
$I_{S,CSR}$
10
20
30
40
N

Fig. 8